JET–P(98)61

T Hellsten et al

# Finite Orbit Width Effects on Ion Cyclotron Heating and Current Drive

JET–P(98)61

# Finite Orbit Width Effects on Ion Cyclotron Heating and Current Drive

T Hellsten[1], J Carlsson[1], L-G Eriksson,
J Hedin[1], M Mantsinen.

JET Joint Undertaking, Abingdon, Oxfordshire, OX14 3EA,
[1]Royal Institute of Technology, Association Euratom-NFR, Stockholm, Sweden.

Preprint of a Paper to be submitted for publication in the proceedings of the
Theory of Fusion Plasmas, Joint Varenna-Lausanne Int. Workshop, Villa Monastero, Varenna,
Italy, August 31 – September 4 1998.

January 1999

## ABSTRACT

Intense ion cyclotron resonance heating can produce anisotropic non-Maxwellian velocity distributions with high energy tails. The distribution functions of the heated ions are determined by wave-particle interactions and Coulomb collisions. A quasi-linear diffusion theory for general wave-particle interaction in a fully toroidal geometry was developed by Kaufmann [1]. In contrast to the theory developed by Stix [2], Kaufmann's quasi-linear diffusion contains diffusion in real space as well as in velocity space. The RF-induced spatial transport as well as the finite orbit width are important for determining the velocity distribution, in particular for small and medium sized devices.

## 1. INTRODUCTION

The damping of magnetosonic waves by ion cyclotron absorption can produce highly anisotropic velocity distributions with very energetic tails. Such tails can strongly enhance the fusion yield, affect the stability of MHD-modes [3], change the absorption and thereby the power partition between the absorbing species. The latter is particularly important for harmonic cyclotron resonance heating for which the absorption of the fast wave by a Maxwellian distribution is in general weak [4]. The development of a non-isotropic velocity distribution may also produce currents, which can be used as central seed currents in bootstrap driven tokamaks, to stabilise MHD-modes [5, 6] and facilitate the formation of transport barriers.

The distribution function of the heated ions can be determined by a Fokker-Planck equation in which the wave-particle interactions are described as a quasi-linear diffusion process. The velocity distributions in the presence of ICRH was first studied by Stix [2]. He derived a 2D-diffusion operator in velocity space, and obtained an analytical solution for a reduced 1D-equation. Subsequently the effects of trapped particles were included in a bounce-averaged Fokker-Planck equation by Kerbel and McCoy [7]. However, these theories were based on the assumption that the drift orbits follow the magnetic surfaces. When modelling ion velocity distributions of RF-heated plasmas, high energy ions in the MeV range were predicted to appear because of the peaked power deposition, and were also observed [8]. However, the predicted energy content of these ions were not always consistent with the experimental observations. For large power levels the deviation becomes stronger and a smaller fast energy content was in general observed than predicted from simple models [9]. These high energy ions move essentially on trapped orbits near the centre with large excursions across the minor radius of the plasma. Explanations of this deviation were put forward in terms of the finite orbit width effects and RF-induced spatial transport. RF-induced spatial transport were discussed by Riyopoulos *et al* [10] and Chen *et al* [11]. The RF-induced spatial transport arises because of the toroidal acceleration of resonating ions interacting with toroidally propagating waves. For an asymmetric wave spectrum this leads to a radial drift similar to the Ware pinch. For symmetric spectra, cancelling the

drift terms, only an RF-induced spatial diffusion remains. They concluded that the RF-induced spatial transport was small and negligible compared with the anomalous particle transport. However, by modelling the problem as a 2D-diffusion, in radius and velocity, it was seen that the RF-induced spatial diffusion during intense ICRH with strongly focused waves had a strong effect on the tail formation [12]. The high energy ions diffused away from the heating region thereby curtailing the formation of a high energy tail, which also resulted in broader power transfer profile. The RF-induced spatial drift appearing for asymmetric toroidal wave spectra can both flatten the power transfer profile or peak it up further depending on the directivity [13].

A quasi-linear diffusion theory for general wave-particle interactions in a fully toroidal geometry, including finite orbit width effects, had been developed by Kaufmann in 1972 [1], but was not until recently applied to ICRH. In Kaufmann's theory the evolution of the distribution function was reduced to a 3D-diffusion equation in a space of invariants of the unperturbed particle motion. In contrast to Stix's theory, Kaufmann's quasi-linear diffusion contains diffusion in real space as well as in velocity space.

Ion cyclotron heating produces high energy ions with most of the energy in the perpendicular component. Such ions make large excursions across the magnetic surfaces. This excursion is here denoted as finite orbit width, which plays an important role for the evolution of the velocity distributions as well as for the power deposition profiles. The finite orbit width effects are important for central heating because of the weak poloidal magnetic field and formation of non-standard orbits, so called potato orbits [14]. As a result of the finite orbit width the collisional power transfer profile is broader than the profile of the absorbed power; because the heated ions absorb power at their Doppler shifted cyclotron resonance but transfer it to the background plasma species all along their orbits. This is further enhanced by the fact that the slowing down is in general faster at the outer part of the orbit where the electron temperature is lower. In small and medium sized devices direct losses due to wide orbits are important [15]. Not only the power transfer but also the absorption is affected by the finite orbit width. Thermonuclear $\alpha$-particles created in the centre of the plasma can absorb power further out because of their wide banana orbits. The details of the velocity distribution is in particular important for current drive where the finite orbit width effects and RF-induced spatial transport give rise to new current drive mechanisms [14-15, 17-18].

Owing to the complexity of the 3D-diffusion problem, solutions have so far mainly been obtained with Monte Carlo codes, which have demonstrated the importance of the RF-induced spatial transport and the finite orbit width [13, 16, 18-20]. Orbit following codes [13, 20] as well as codes calculating the orbit averaged distribution function [14] have been developed. An effort to solve the 3D-equation with a finite difference method has also been made [21].

First experimental evidence of an RF-induced drift of trapped ions has recently been reported from JET showing a strong effect on the neutral particle spectra, excitation of TAE-

modes and ELMs [23]. In Tore Supra and DIII-D asymmetry in the current drive efficiency during fast wave current drive have been observed [24, 25] being consistent with the different tails formed for the different phasings [22].

## 2. QUASI-LINEAR DIFFUSION IN A TORUS

The quasi-linear theory was originally developed to calculate the saturation of wave fields driven by micro instabilities. It is based on the assumption that the amplitudes of a set of uncorrelated waves are small, so that the zero order distribution function evolves on a slow time scale compared to a wave period. For ICRH the wave field consists of a correlated set of Fourier modes driven by an antenna. However, the theory can still be applied if one assumes the gyro phase of the particle to be decorrelated by Coulomb collisions or non-linear effects [26-28] between the different interactions. Since the collision frequency and the time to change the energy by wave-particle interactions are long compared to the bounce time. It is possible to perform a multiple time scale expansion of the distribution function in which the slowly varying component of the distribution function is a function of the three invariants only [1]. Thus, the diffusion is reduced to 3-dimensions.

In an axisymmetric toroidal geometry the guiding centre trajectories are integrable implying that invariants describing the orbits can be found. A particle will stay on its guiding centre orbit, if it is not subjected to collisions or wave-particle interactions and if its orbit does not intersect the wall or any another obstacle. To describe an orbit we use the invariants ($E$, $P_\phi$, $\Lambda$) [29], where $E$ is the energy, $P_\phi = Rmv_\phi + eZ\psi(r)$ is the canonical angular momentum and $\Lambda = B_0\mu/E$ is an adiabatic invariant , defined by the ratio between the magnetic moment and energy normalised with the respect to the magnetic field at the magnetic axis. There is not a unique relationship between these invariants and the orbits; the same triple may describe different types of orbits. To distinguish between them, a label $\sigma$ is introduced. To classify the orbits, it is useful to separate the invariant space ($E$, $P_\phi$, $\Lambda$) into nine regions [30] as illustrated in Fig. 1. In the regions I-IV two solutions exist, in the regions V-VIII only one solution exists and in region IX there is no solution. During ICRH the number of ions with non-standard orbits appearing in regions III-IV and VIII is increased because of the preferential perpendicular heating.

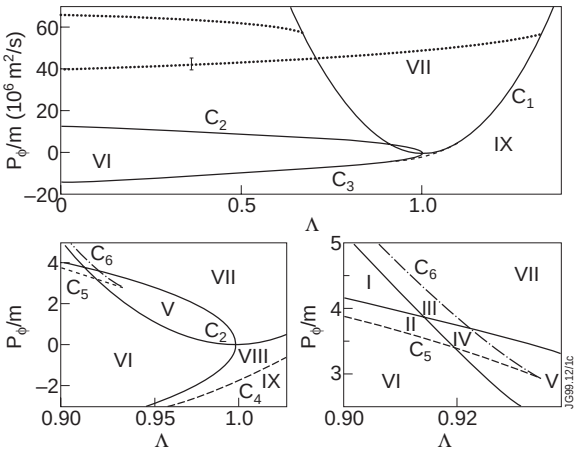


*Fig. 1 The invariant space of a 100keV proton.*

Wave-particle interactions and Coulomb collisions will break the invariants and cause a random walk in the invariant space. Thermal ions will be subjected to a rather rapid energy

diffusion and pitch angle scattering with other ions which will tend to isotropise and produce nearly Maxwellian distribution functions. For highly energetic ions, the Coulomb collisions with other ions become negligible. The ions will instead lose their energy to the electrons by a non-diffusive process [2]. The energy of the resonating ions are determined by the balance between absorbed power by wave-particle interactions and power transferred to the background plasma species. As a thermal resonating ion is gradually heated by cyclotron damping, it will on the average increase its perpendicular energy and as a consequence the orbit will turn into a trapped one. As the particle is further heated, the turning point of the trapped orbit will drift vertically along the cyclotron resonance. When the cyclotron resonances passes through the magnetic axis the radial drift with respect to minor radius, $v_T$, is given by

$$v_T = \sum_{n_\phi} \frac{n_\phi q p\left(n_\phi\right)}{m \omega \omega_{ci} r}, \tag{1}$$

where $p$ denotes the absorbed power per particle for a given toroidal mode number $n_\phi$. For waves propagating in the opposite direction as the plasma current, the banana tips of the ion orbits will drift vertically outwards along the cyclotron resonance. These ions will then either hit the wall or be thermalised as they move into a region with lower wave field strength. If the wave propagates in the same direction as the plasma current, the turning point of the ions will drift vertically inwards along the cyclotron resonance. As the turning points approach the mid plane, the orbits will turn into passing orbits or into potato orbits or counter passing orbits lying on the low field side of the magnetic axis not encircling the magnetic axis. Which of these orbits they will turn into depends on the position of the cyclotron resonance and their energy.

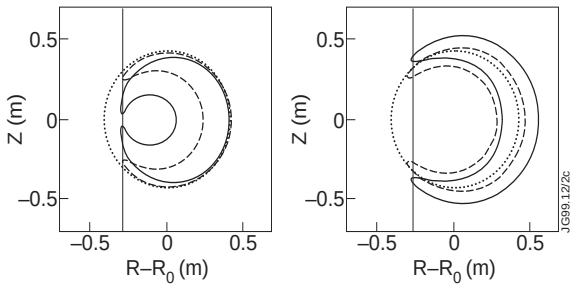


*Fig. 2. Two drift orbit after 0 s (dotted), 0.2 s (dashed), and 1.3 s (full) of heating, $n_\phi$ =15 (right hand side) and $n_\phi$ =-15 (left hand side). The vertical line is the cyclotron resonance.*

For a symmetric spectrum, cancelling the drift terms, the trapped high energy ions diffuse radially away from the region of intense wave-particle interactions due to the large density gradient of high energy ions and the relatively high diffusion coefficient for these ions. In the limit of small Larmor radius $\rho_i$, $\left(k_\perp \rho_i << 1\right)$ and for heating at the fundamental cyclotron frequency the RF-induced radial diffusion coefficient for the turning point of the trapped ions is given by

$$D_T = \sum_{n_\phi} \frac{2p\left(n_\phi\right)}{m} \left( \frac{v_\perp n_\phi q}{\omega \omega_{ci} r} \right)^2 . \tag{2}$$

The evolution of the orbit averaged distribution function, *f*, of the heated ions can be calculated by deriving a Fokker-Planck equation. Since in a toroidal geometry the parallel and perpendicular velocities vary along the orbit, which couples the space and velocity variables, it is convenient to express the diffusion equation for the orbit averaged distribution function in the space of orbit invariants [1, 31]

$$\frac{\partial f}{\partial t} = \langle Q \rangle(f) + \langle C \rangle(f), \tag{3}$$

where $\langle Q \rangle$ is the orbit averaged quasi-linear RF-operator and $\langle C \rangle$ the Coulomb diffusion operator. Eq. (3) can then be written in the form

$$\frac{\partial f}{\partial t} = \frac{1}{\sqrt{g}} \frac{\partial}{\partial I_i} \cdot \left[ \sqrt{g} \left( a_{Ci}\ f + \left( D_{Cij} + D_{RFij} \right) \cdot \frac{\partial f}{\partial I_j} \right) \right], \tag{4}$$

where $\sqrt{g}$ is the Jacobian and $I_i$ the invariants. The orbit averaged distribution function can also be obtained by calculating the changes of the invariants over the unperturbed orbits of test particles and then solving the corresponding stochastic Langevin equation with a Monte Carlo method. The distribution function is then obtained as a set of points in the invariant space. These two approaches are equivalent [31]. The orbit averaged Monte Carlo increments can either be calculated directly [32] or be derived from the orbit averaged Fokker-Planck equation [31].

When averaging over the gyro phase, the Coulomb collisions are described as scattering in a local $(v_\perp, v_\parallel)$-space at each position along the guiding centre orbit. Locally the collisions will scatter the invariants along a surface in the invariant space. The surface depends on the position of the collision and thus produce a 3D-diffusion in the invariant space. Scattering of trapped ions and between trapped and passing leads to neo-classical diffusion.

The changes in the invariants due to wave-particle interactions are given by

$$\Delta E = \frac{eZv_{res\perp}}{m} \left| E_+ J_{n-1}(k_\perp \rho_L) + E_- J_{n+1}(k_\perp \rho_L) \right| \sqrt{\frac{2\pi m}{n\ |\ \dot{\omega}_c\ |}} \cos\varphi,$$

$$\Delta\Lambda = \frac{2\left(n\omega_{c0} - \Lambda\omega\right)}{\omega E} \Delta E, \qquad \Delta P_\phi = \frac{n_\phi}{\omega} \Delta E, \tag{5}$$

where $\varphi$ is the difference between the gyro phase of the particle and the phase of the wave and $v_{res\perp}$ is the perpendicular velocity at the Doppler shifted cyclotron resonance. For high energy ions, it is important to keep the $E_-$-component of the electric field and the unexpanded Bessel functions. The terms within the bracket in Eq. (5) may cancel, leading to an effective barrier for diffusion in the velocity space [33]. In the case $\dot{\omega}_c = 0$, i. e. when the turning point of the orbit coincides with the cyclotron resonance, the variation of the gyro phase has to be expanded to higher order. In this case $\Delta E$ can be expressed in terms of Airy functions [7]. The RF-interaction

for a single frequency and a single toroidal mode number represents a one dimensional diffusion in the invariant space. The wave-particle interactions if not decorrelated should be calculated by adding the interactions by the different wave numbers in a correlated wave, since the wave field and hence the changes in phase between the different wave interactions are uniquely determined by the current distribution in the antenna. The time between the interactions for the different $n_\phi$ are in general too short to be decorrelated by Coulomb collisions; this is particularly important for particles which are close to tangency resonance i. e. $\dot{\omega}_c = 0$. However, the interactions can be decorrelated by non-linearities.

The Langevin equation is not uniquely determined, an equation for the changes in $E$, $P_\phi$ and $\Lambda$ is given by [34]

$$\begin{bmatrix} E(t+\Delta t) \\ \Lambda(t+\Delta t) \\ P_\phi(t+\Delta t) \end{bmatrix} = \begin{bmatrix} E(t) \\ \Lambda(t) \\ P_\phi(t) \end{bmatrix} + \begin{bmatrix} \dot{\mu}_C^E \\ \dot{\mu}_C^\Lambda \\ \dot{\mu}_C^{P_\phi} \end{bmatrix} \Delta t + \begin{bmatrix} \dot{\mu}_{RF}^E \\ \dot{\mu}_{RF}^\Lambda \\ \dot{\mu}_{RF}^{P_\phi} \end{bmatrix} \Delta t +$$
$$+ \begin{bmatrix} X_{1C} & 0 & 0 \\ 0 & Y_{2C} & 0 \\ Z_{1C} & Z_{2C} & Z_{3C} \end{bmatrix} \begin{bmatrix} \zeta_{1C} \\ \zeta_{2C} \\ \zeta_{3C} \end{bmatrix} \sqrt{\Delta t} + \begin{bmatrix} X_{1RF} & 0 & 0 \\ Y_{1RF} & Y_{2RF} & 0 \\ Z_{1RF} & Z_{2RF} & Z_{3RF} \end{bmatrix} \begin{bmatrix} \zeta_{1RF} \\ \zeta_{2RF} \\ \zeta_{3RF} \end{bmatrix} \sqrt{\Delta t} \tag{6}$$

The expectation values are defined by $\dot{\mu}_i \Delta t = \langle\langle \Delta I_i \rangle\rangle$, $\zeta_i$ are random numbers with unit variances and zero expectation values, $X_i$, $Y_i$ and $Z_i$ are given by

$$X_1 = \sqrt{\dot{\sigma}_{EE}\Delta t}, \quad Y_1 = \frac{\dot{\sigma}_{\Lambda E}\Delta t}{\sqrt{\dot{\sigma}_{EE}\Delta t}}, \quad Y_2 = \sqrt{\dot{\sigma}_{\Lambda\Lambda}\Delta t - Y_1^2}, \quad Z_1 = \frac{\dot{\sigma}_{P_\phi E}\Delta t}{\sqrt{\dot{\sigma}_{EE}\Delta t}},$$
$$Z_2 = \left(\dot{\sigma}_{P_\phi \Lambda}\Delta t - Y_1 Z_1\right) \sqrt{\dot{\sigma}_{\Lambda\Lambda}\Delta t - Y_1^2}, \quad Z_3 = \sqrt{\dot{\sigma}_{P_\phi P_\phi}\Delta t - Z_1^2 - Z_2^2} \tag{7}$$

where $\dot{\sigma}_{ij}\Delta t = \left\langle\left\langle \left(\Delta I_i - \dot{\mu}_i \Delta t\right)\left(\Delta I_j - \dot{\mu}_j \Delta t\right)\right\rangle\right\rangle$ define the variances and the covariances. The double bracket $\langle\langle ... \rangle\rangle$ denotes averaging locally and along the orbit. The averaging includes also weighting over the toroidal and the poloidal mode number spectra. A dot on top of a variable denotes the total time derivative. In general, the changes in the invariants due to collisions and wave-particle interactions vary quite smoothly within the different regions in the space of invariants, but may change more rapidly near the boundaries. The expectation values and variances are related to $D_{ij}$ and $a_i$ in Eq. (3) by [31]

$$\dot{\mu}_i = -a_i + \frac{1}{\sqrt{g}} \frac{\partial}{\partial I_j}\left(\sqrt{g} D_{ij}\right) \text{ and } \dot{\sigma}_{ij} = D_{ij} + D_{ji} = 2D_{ij}. \tag{8}$$

## 3. TAIL FORMATION

Information on the high energy tail produced by ICRH can be observed from various diagnostics. In steady state the fast energy of the heated ions is given by

$$W_{fast} = \frac{p_e t_s}{2}, \tag{9}$$

where $p_e$ is the power transferred to the electrons and $t_s$ is Spitzer's slowing-down time [2]. Deviations may be caused by that high energy ions passing through the outer region with a lower electron temperature. They will slow down faster and at the same time broadening the power transfer profile. For wide orbits the slowing down time has to be averaged over the particle trajectories. The RF-induced spatial transport has also a strong effect on the tail formation, which can be rather different for low and high $n_\phi$ -spectra. For modest power levels good agreements between $W_{\text{fast}}$ deduced from experimental measurements and estimates of Eq. (9) is often obtained. However, at higher power levels discrepancies appear. When the slowing down time is averaged over the orbits, better agreements are obtained [9]. How the fast energy content agrees with more advanced 3D-calculations of minority heating scenarios with constant temperature and density profiles made with the FIDO-code [15] can be seen in Fig. 3. The FIDO code computes the orbit averaged distribution function in terms of the invariants ($E$, $P_\phi$, $\Lambda$). The total energy distribution functions, neglecting the RF-induced spatial transport and the wide orbits, agree fairly well with those obtained from thin orbits. The latter were obtained by choosing a high plasma current which agreed fairly well with the Stix's solutions except at very high energies (Fig. 3). The spatial variation of the energy distribution of the heated ions deviates considerable from the thin orbit model. For symmetric low $|n_\phi|$ - spectra the orbit width effects dominate whereas for high $|n_\phi|$-spectra the RF-induced spatial diffusion becomes important. This can be seen by studying the energy spectra of ions impinging the wall as shown in Fig. 4 [15]. For low $|n_\phi|$ the turning points of the trapped ions remain fairly unchanged. A fraction of these ions will be heated up until they hit the wall; this results in a degradation of the heating efficiency coming from the losses of high energy ions. For high $|n_\phi|$ the heated high energy ions will diffuse away from the centre and a fraction of them hits the wall but with a lower energy than for low $|n_\phi|$. The spatial transport of high energy particles becomes stronger and more important for asymmetric spectra.

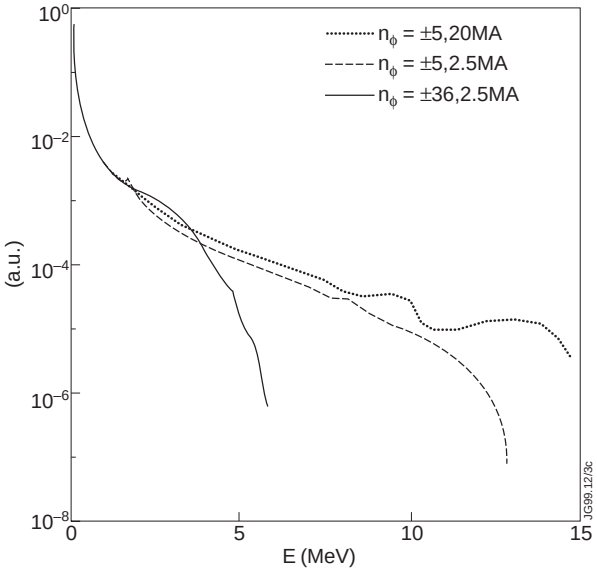


*Fig. 3. Global energy spectra of resonant ions.*

The confinement of the high energy ions is particularly important for heating at higher harmonics for which the cyclotron absorption

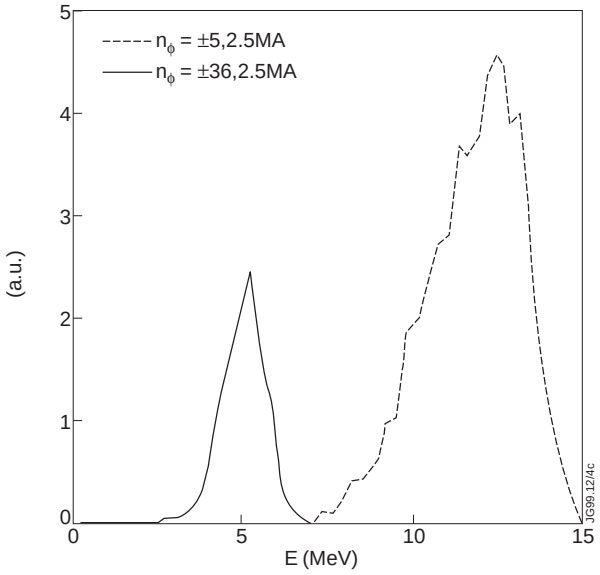


*Fig. 4. Energy spectra of ions impinging the wall*

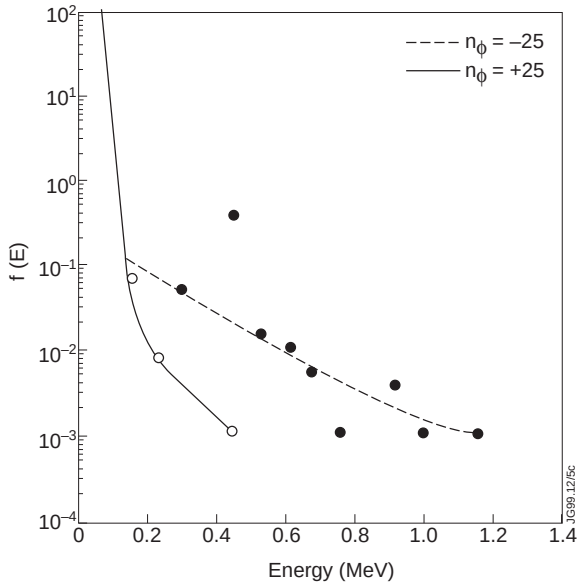


*Fig. 5. Energy distribution for different phasings $n_\phi$=25 (full) and $n_\phi$=-25 (dotted).*

for thermal ions is weak, the total absorption by the ions depends then strongly on the confinement of high energy ions [4]. If the drift is directed inwards, the high energy ions can be confined whereas if it is directed outwards, the confinement is reduced. In Fig. 5 the energy distributions for different phasings during third harmonic heating of deuterium are shown, for parameters given in Ref. [22] similar to those used in some current drive experiments in Tore Supra [24].

## 4. MINORITY CURRENT DRIVE

Minority ion current drive, originally proposed by Fisch [35], is obtained by coupling toroidally directed waves. The absorption takes place at different locations in real space and velocity space due to the resonance condition $\omega = n\omega_c + k_{||}v_{||}$. Owing to the localised diffusion in velocity space and the energy dependence of the Coulomb collision frequency the perturbation of the distribution function at low energies will be smoothed out faster than at high energies resulting in a net ion current. For a magnetic field decreasing with the major radius, a bi-directional ion current around the cyclotron resonance is formed. In the Fisch model of minority current drive neither the absorption of the waves toroidal angular momentum, the RF-induced spatial transport, the trapping and the orbit width effects are accounted for. Since ICRH produces ion tails with a large fraction of trapped ions, these effects are therefore expected to become important; when including them new mechanisms forming the current appear. The wave interaction takes place at the Doppler broadened cyclotron resonance determined by $k_{||}$ whereas the RF-induced drift depends on $n_\phi$. For Fourier modes with high $|m|$ the sign of $k_{||}$ and $n_\phi$ can even be different. The importance of the RF-induced spatial drift and the finite orbit width effects can be seen by comparing the predicted current drive density from the Fisch theory with the FIDO-code for high plasma currents for which the finite orbit width effects can be neglected. The comparison

shows good agreement for low power levels as seen in Fig. 6 [19]. However, as the wave field is increased the deviation from the Fisch model essentially arises because of trapped particles are created with high power densities. For lower plasma currents the bi-directional current created by trapped ions and the RF-induced drift dominates the formation of the current. The back current carried by electrons and the back ground ion species are not included in Fig. 6, but can be included by locally correcting the minority current density [36].

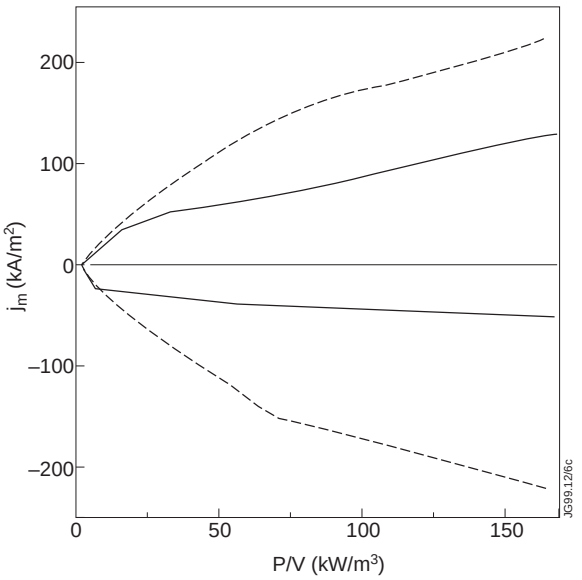


*Fig. 6. Comparison of the current integrated around two flux surfaces, r = 25 cm (top) and at r = 35 cm (bottom), versus the absorbed power inside these pairs of flux surfaces.FIDO-code (solid) and Fisch model (dashed). The resonance surface is at $R_c$=30 cm.*

The non-standard orbits in the centre produce a current even for symmetric spectra [14, 17]. This current can be used as a central seed current in a bootstrap current driven tokamak. By using $n_\phi < 0$ and heating the $\alpha$-particles in the centre a relative large seed current is obtained [19]. Through this article the geometry has been chosen so that the plasma current is negative. For $n_\phi < 0$ the wave is propagating in the same direction as the plasma current resulting in that the turning points of the trapped high energy ions drift along the cyclotron resonance towards the mid plane and detrap into ions with co- and counter-passing orbits as discussed in section 2. If the cyclotron resonance is located on the high field side of the magnetic axis, trapped ions having their turning points close to the mid plane will scatter into co- and counter orbits producing a bi-directional ion current. If the cyclotron resonance passes close to the magnetic axis, potato shaped orbits will be formed for high energy ions which will preferentially scatter into counter-passing orbits [19]. When the cyclotron resonance passes at the low field side of the magnetic axis, the trapped ions turn into counter passing orbits in region VIII in the ($E$, $P_\phi$ $\Lambda$)-space as shown in Fig. 1. Although the transition of the orbits from one type to an other takes place directly, the current distribution associated with the orbit changes continuously due to the precession of the orbits. For these scenarios a net negative current is

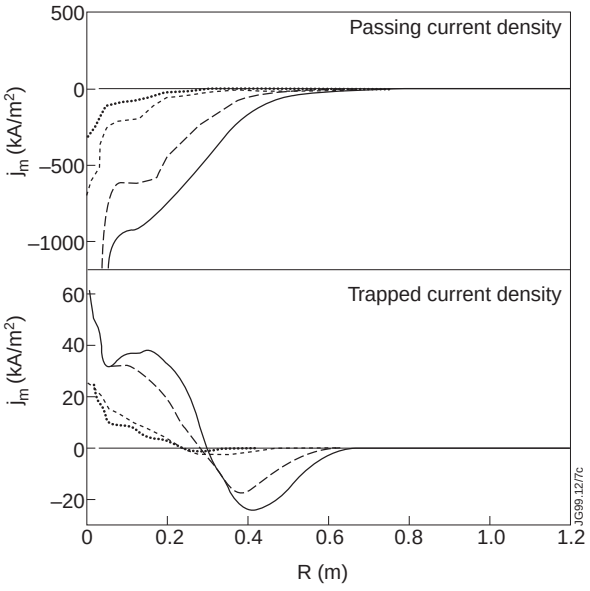


*Fig. 7. Current drive for on-axis resonance $n_\phi$=-15, at different levels of coupled powers (0.6, 1, 5 and 10MW) for JET like parameters [18].*

produced with respect to the plasma current. In Fig. 7 the current densities from trapped and passing ions are illustrated. For $n_\phi > 0$ the trapped ions drift outwards which can almost completely curtail the tail formation. However, if the power density is sufficiently high, a bi-directional current is obtained caused by the trapped ions, due to the precession drift a net current appears. For symmetric spectra the drift terms only partly cancel because of the peaked wave profiles and that the wave-particle interactions take place at different flux-surfaces.

## 5. THE EFFECT OF THE FINITE ORBIT WIDTH ON THE WAVE ABSORPTION

Although the finite orbit width and RF-induced transport can substantially affect the local distribution function and in particular the high energy part, the change in the absorption may not be as spectacular. This depends on the relative change of the anti-Hermitian part of the dielectric tensor. If the tail particles are few, the modifications may be small. Often the main effect comes from modifications of the distribution function just above the thermal velocity. By increasing the parallel velocity distribution the width of the resonance layer increases, and in the case of minority heating at the fundamental cyclotron resonance the absorption often improves. For second harmonic heating the absorption is increased, if a perpendicular tail is formed. High energy ions like $\alpha$-particles making large excursion across the plasma radius may absorb power on flux surfaces where they are not created. To calculate the absorption in a volume element, the contributions to the dielectric tensor from all resonating ions passing through this element have to be included, which become more complicated, if a non-local distribution function expressed in terms of orbit invariants is used. This is the case when the distribution function is obtained by solving the orbit averaged distribution function with a Monte Carlo code, such as FIDO. The local velocity distribution has then to be evaluated from a set of orbits. This can be done by adding contributions to all fluid elements in phase space ($\underline{r}$, $\underline{v}$) for which each orbit passes through. Expressing these contributions in finite element basis functions $\phi_j(v_\parallel)$ and $\varphi_k(v_\perp)$ one obtains

$$f(\underline{r},\underline{v}) = \sum a_{kj}(\underline{r})\,\varphi_k(v_\perp)\phi_j(v_\parallel). \qquad (10)$$

The derivatives appearing in the susceptibility tensor elements are obtained in a similar way by expressing them in terms of the derivatives of the basis functions

$$\frac{\partial f(\underline{r},\underline{v})}{\partial v_\perp} = \sum a_{kj}(\underline{r})\frac{\partial \varphi_k(v_\perp)}{\partial v_\perp}\phi_j(v_\parallel) \quad \text{and} \quad \frac{\partial f(\underline{r},\underline{v})}{\partial v_\parallel} = \sum a_{kj}(\underline{r})\,\varphi_k(v_\perp)\frac{\partial \phi_j(v_\parallel)}{\partial v_\parallel} \quad . \qquad (11)$$

Using the susceptibility tensor for the resonating ions, given for an arbitrary velocity distribution in a homogenous plasma for propagating plane waves (see e. g. [26] ), the absorption by the high energy ions can be included by using the local dispersion relation for $k_\perp$ in the argument of the Bessel functions [37]. For high energy ions it is important to keep the unexpanded Bessel functions in the dielectric tensor since their Larmor radii can become comparable with the wave length of the fast wave. In particular for high energy ions the contributions from the $E_+$ and $E_-$ terms sometimes nearly cancel [33].

The susceptibility tensor expressed in a local orthogonal coordinate system ($x$, $y$, $z$), where $z$ is along the magnetic field and $y$ chosen so that $k_y = 0$, is given by

$$\underline{\underline{\chi}}_{\alpha} = \frac{2\pi\omega_{p\alpha}^2}{\omega}\int_0^{\infty} v_{\perp}^2 dv_{\perp}\int_{-\infty}^{\infty} dv_{\parallel}\left\{\left[\frac{\partial f}{\partial v_{\perp}} + \frac{k_{\parallel}}{\omega}\left(v_{\perp}\frac{\partial f}{\partial v_{\parallel}} - v_{\parallel}\frac{\partial f}{\partial v_{\perp}}\right)\right]\sum_{n=-\infty}^{\infty}\frac{\underline{\underline{T}}_n}{\omega - k_{\parallel}v_{\parallel} - n\omega_{c\alpha}}\right\}_{\alpha} \quad (12)$$

where $\underline{\underline{T}}_n = \begin{bmatrix} \frac{n^2 J_n^2}{z^2} & \frac{inJ_nJ_n'}{z} \\ -\frac{inJ_nJ_n'}{z} & (J_n')^2 \end{bmatrix}$

and $J_n(z)$ with the argument $z = k_{\perp}v_{\perp}/\omega_{c\alpha}$. The acceleration by a parallel electric field is not included. To reduce the fluctuations caused by using a finite number of orbits when numerically evaluating $\underline{\underline{\chi}}_{\alpha}$, the fluid elements have to be sufficiently large.

Assessment of the absorption by thermonuclear $\alpha$-particles using the above method has been done in Ref. [37] for second harmonic heating of tritium in a JET plasma, where some of the $\alpha$-particles produced in the centre make large excursions across the plasma and may absorb power at their Doppler shifted second harmonic resonance near the edge. The contributions of the resonating ions to the dielectric tensor were added as described above and the wave field calculated with the LION code [39-40]. The absorption by the $\alpha$-particles near the boundary turned out to be negligible due to higher order Larmor radius effects, but became significant at the fundamental resonance at the high field side.

How the RF-induced spatial drift affects the absorption through differences in the high energy tails in the distribution functions can be illustrated by studying absorption at the third harmonic deuterium resonance. This absorption appears as a parasitic absorption during fast wave current drive by direct electron damping and has been shown to be important when the tail ions are confined [4]. To show how the absorption is affected by the differences in the tails due to different radial drift caused by different toroidally directed waves, we plot the increase in single pass absorption normalised to a Maxwellian one for different toroidal mode numbers in Fig. 8. The parameters have been chosen similar to those in Tore Supra given in Ref. [22].

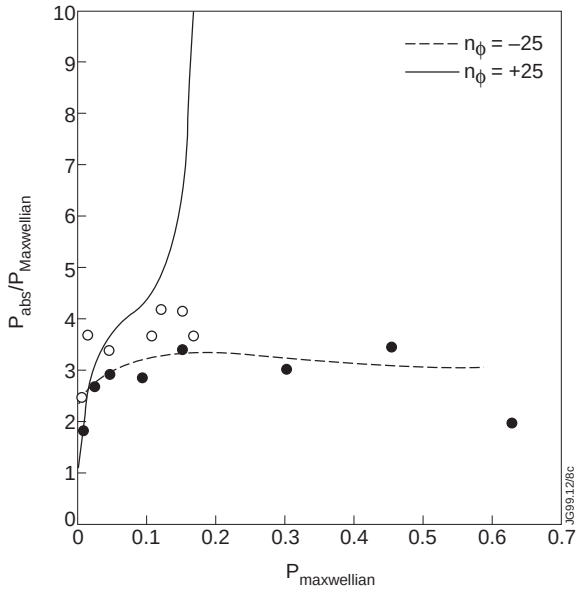


*Fig. 8. Ratio of absorbed power for the computed distribution function and a Maxwellian versus power absorbed by the Maxwellian, for different phasings $n_\phi$=25 (full) and $n_\phi$=-25 (dotted).*

Because the velocity distribution of the heated ions strongly affects the power deposition, self-consistent calculations of the power deposition and velocity distribution have to be done to assess the impact of ICRH during fast wave current drive where parasitic third harmonic cyclotron absorption on deuterium takes place. Calculations of the wave field including these effects using the SELFO-code have been done in Ref. [22] including orbit width effects and RF-induced transport. In this case the confinement of the tail is of utmost importance for calculating the wave field and the power partition. The dependency of the confinement of fast ions on the directivity of the fast wave is consistent with the observed asymmetry of the current drive [24-25]. The increase of the single pass damping changes the wave field from one being weakly damped, which is well spread over the plasma cross section, to one strongly damped, which is focused close to the magnetic axis.

## 6. SUMMARY

The large excursions of the drift orbits across the magnetic surfaces are important for the evolution of the velocity distribution of ions heated by ICRH. The absorption profiles for high energy ions like thermonuclear $\alpha$-particles, created in the centre of the plasma, can absorb power further out due to the wide banana orbits. The collisional power transfer profiles are broader than the profile of the absorbed power.

Owing to the toroidal acceleration of resonating ions interacting with toroidally propagating waves, the quasi-linear RF-diffusion results in diffusion in real space as well as in velocity space. For a toroidally directed wave spectrum a radial drift similar to the Ware pinch appears. For symmetric spectra for which the drift terms cancel only an RF-induced spatial diffusion remains.

In small and medium sized devices prompt losses due to wide orbits lead to a reduction in the heating efficiency. These losses can become devastating for heating in smaller machines with low plasma current and may be one of the reasons why ICRH was not efficient until experiments with sufficient high plasma current such as in PLT and TFR became available.

The estimate of the fast energy of the heated ions given by Eq. (9) often overestimates the fast energy. A first correction is obtained by averaging the slowing down time over the trajectories of the particles. The RF-induced spatial transport can also have a strong effect on the tail formation in particular for asymmetric high $n_\phi$ -spectra.

Because ICRH produces at typical experimental parameters large perpendicular ion tails with a large fraction of trapped ions, the effects of the finite orbit width and the RF-induced spatial drift result in new current drive mechanisms.

Although the finite orbit width and RF-induced transport can substantially affect the local distribution function and in particular the high energy part, the change in the absorption may not be as spectacular. The RF-induced spatial transport affects the confinement of high energy ions and becomes particularly important for heating at higher harmonics for which the absorption is

in general weak. When modelling high energy tail and the absorption by high energy particles it is important to keep the Bessel functions unexpanded in the dielectric tensor.

Because the velocity distribution of the heated ions strongly affects the power deposition, self-consistent calculations of the power deposition and velocity distribution have to be done in order to assess the impact of ICRH. For many heating scenarios, in particular for heating and current drive in smaller machines, the effects of finite orbit width and the RF-induced spatial transport have to be included.

Experimental evidence of an RF-induced drift has been reported from JET showing a strong effect on the neutral particle spectra, excitation of TAE-modes and ELMs [23]. In Tore Supra an asymmetry in the current drive efficiency during fast wave current drive has been observed [24-25] being consistent with the different tails formed for the different phasings [22]. Experimental evidence of the importance of higher Larmor radius corrections for the high energy tails has recently been reported from JET [33].

**REFERENCES**


[1] A. N. Kaufmann, Phys. Fluids **6**(1972)1063.

[2] T. H. Stix, Nuclear Fusion **15**(1975)737.

[3] F. Porcelli *et al.*, Proc. of Inter. Conf. on Plasma Physics, Innsbruck, 1992, Vol.16C, Pt. II, p. 901.

[4] L.-G. Eriksson *et al.*, Nuclear Fusion, **38**(1998)265.

[5] D. F. H. Start, *et al.*, Proc. of Inter. Conf. on Plasma Physics, Innsbruck, 1992, Vol. 16 C, Pt. II, p. 897.

[6] V. P. Bhatnagar, et al, Nucl. Fusion **34**(1994)1579.

[7] G. D. Kerbel and M. G. McCoy, Phys Fluids **28**(1985)3629.

[8] J. M. Adams *et a*l., Nuclear Fusion **31**(1991)891.

[9] L.-G. Eriksson, *et al*., in Proc. of Theory of Fusion Plasmas, Varenna, 1994, 101.

[10] S. Riyopoulos *et al.*, Nucl. Fusion **26**(1986)627.

[11] L. Chen, J. Vaclavik and G. W. Hammett, Nuclear Fusion **28**(1988)389.

[12] T. Hellsten, Plasma Physics and Controlled Fusion **31**(1391)1989.

[13] M. A. Kovanen, W. G. F. Core, T. Hellsten, Nuclear Fusion **32**(1992)787.

[14] L.-G. Eriksson, *et al*, 1992 Int. Conf. on Plasma Physics, Innsbruck, 1992, Vol. II, p. 1469.

[15] J. Carlsson, L.-G. Eriksson and T. Hellsten, Nuclear Fusion **37**(1997)719.

[16] J. Carlsson, *et al.*, in Proc. of Theory of Fusion Plasmas, Varenna, 1994, 351.

[17] W. G. F. Core and G. A. Cottrell, Nuclear Fusion **32**(1992)1637.

[18] T. Hellsten, J. Carlsson and L.-G. Eriksson, Phys. Rev. Lett. **74**(1995)3612.

[19] J. Carlsson and T. Hellsten, and J. Hedin, Physics of Plasmas **5**(1998)2885.

[20] J. A. Heikkinen and S. K. Sipilä, Nuclear Fusion **37**(1997)835.

[21] F. S. Zaitsev, M. R. O'Brien and M. Cox, Physics of Fluids **B5**(1993)509.

[22] J. Hedin, T. Hellsten and J. Carlsson, this conference.
[23] L.-G. Eriksson *et al.,* Phys. Rev. Lett. **81** (1998)1231.
[24] B. Saotic *et al.*, Plasma Physics and Controlled Fusion **36**(1994)B123.
[25] R. Prater *et al*, in Proc. 16th IAEA Fusion Energy Conference, Monteral, Canada 1996, Vol. III, p. 243.
[26] T. H. Stix, *Waves in Plasmas*, AIP, New York, 1992.
[27] A. Bécoulet, D. Gambier and A. Samain, Physics of Fluids **B3**(1991)137.
[28] P. Helander and M. Lisak, Physics of Fluids **B4**(1992)1927.
[29] J. A. Rome and Y.-K. M. Peng, Nucl. Fusion **19**(1979)1193.
[30] F. Porcelli *et al.*, Proc. of 21st EPS. Conf. on Controlled Fusion and Plasma Physics, Montpellier, 1994, Vol II, p. 648.
[31] L.-G. Eriksson and P. Helander, Physics of Plasmas **1**(1994)308.
[32] J. Carlsson, L.-G. Eriksson and T. Hellsten, ALF-1996-104, Alfvén Laboratory, Royal Institute of Technology, SE-100 44 Stockholm, Sweden.
[33] M. J. Mantsinen, *et al.*, to appear in Nuclear Fusion.
[34] S. Putvinskii and B. Tubbing, JET Report, JET-R(93)03, JET Joint Undertaking, Abingdon, Oxon, OX143EA, UK.
[35] N. J. Fisch, Nucl. Fusion **21**(1981)15.
[36] J. W. Connor and J. G. Cordey, Nucl. Fusion **14**(1974)185.
[37] J. Hedin, *et al.,* Plasma Physics and Controlled Fusion **40**(1998)1037.
[38] L.-G. Eriksson, *et al.*, Phys. of Plasmas **6**(1999)513.
[39] L. Villard *et al*., J. Comput. Phys. Rep. **4**(1986)95.
[40] L. Villard *et al*., Nuclear Fusion **35**(1995)1173.